Progress In Electromagnetics Research, PIER 101, 157–171, 2010

DESIGN AND EXPERIMENTS OF THE GW HIGH-POWER MICROWAVE FEED HORN

C. Chang

Department of Engineering Physics
Tsinghua University
Beijing, China

X. X. Zhu, G. Z. Liu, J. Y. Fang, R. Z. Xiao, C. H. Chen H. Shao, J. W. Li, H. J. Huang, and Q. Y. Zhang

Northwest Institute of Nuclear Technology
Xi'an, Shannxi, China

Z. Q. Zhang

National Key Laboratory of Antennas and Microwave Technology
Xidian University
Xi'an, Shannxi, China

Abstract—Design and optimization of high-power microwave (HPM) feed horn by combining the aperture field with radiation patterns are presented in the paper. The optimized feed horn in C band satisfies relatively uniform aperture field, power capacity higher than 3 GW, symmetric radiation patterns, low sidelobes, and compact length. Cold tests and HPM experiments were conducted to investigate the radiation patterns and power capacity of the horn. The theoretical radiation patterns are consistent with the cold test and HPM experimental results. The power capacity of the compact HPM horn has been demonstrated by HPM experiments to be higher than 3 GW.

1. INTRODUCTION

The maximum power produced by S-band resonant BWO has attained 5 GW with 100 J energy pulses [1]. With the development of narrowband multi-giga-watt HPM sources operated under vacuum, the power capacity of the HPM horn has become the major factor of

Corresponding author: C. Chang (changc02@mails.tsinghua.edu.cn).

limiting HPM transmission and radiation [2–5]. When the electric field amplitude at the aperture of the horn is higher than the breakdown threshold, secondary electron multipactor and plasma discharge happen at the vacuum side of the dielectric radome, leading to HPM breakdown and pulse shortening [2–5]. Consequently, in order to prevent breakdown, the aperture field of HPM horn should be uniform and below the breakdown threshold, which is about 30–40 kV/cm for S-X band HPM [6]. The aperture diameter Φ of the horn usually requires 0.8–1 m for the power capacity higher than 3 GW. Besides, as a feed of the reflected antenna, the HPM feed horn need symmetric radiation patterns and low sidelobes. Thus, it is very important to choose and design HPM horn satisfying high power capacity and symmetric radiation patterns.

There are varied horns applied for special occasions: single-dominant mode conical and rectangular horn [7–11, 24, 25], multimode circular and rectangular horn [12–15], corrugated horn [11, 16], modified box-horn [17, 18], half oval horn [19], ridged-loaded UWB horn and modified TEM horn [20–22].

For the narrowband HPM, the power capacity of the circular horn with the same aperture size is higher than that of the rectangular horn whose the aperture field is less uniform. Dominant-mode TE_{11} conical horn has uniform aperture field, but demands small flare to neglect the higher-mode field components [9], leading to a long length $L \sim 2$–3 m for HPM horn with $\Phi \sim 0.8$–1 m. More importantly, TE_{11} conical horn has non-symmetric radiation patterns and is not suitable to be a high efficient feed horn.

Corrugated horn has the advantage of symmetric patterns and low sidelobes [7–9]. However, the corrugated horn with $\Phi \sim 0.8$–1 m and length $L \sim 1$ m has a weight of several tons even for the aluminum material, leading to difficult processing and expensive cost. What's more, the bottleneck of the power capacity of the corrugated horn is at the section of smooth waveguide flaring to the corrugated wall with small diameter, where the field between the slots is so strong that discharge occurs violently.

Unfortunately, the importance of the aperture field amplitude has been neglected in the design of the HPM feed horn in Ref. [23], whose power capacity is still not investigated by HPM experiment. Besides, the feed horn in Ref. [23] with $L = 1.45$ m and $\Phi = 0.4$ m is not compact.

In this paper, we propose to design and optimize HPM feed horn according to the way of combining the aperture field with radiation patterns. A two-time flared circular feed horn in C band is optimized by CST Microwave Studio [26]. Cold test and 3 GW HPM

experiment were conducted to investigate the radiation patterns and power capacity of the horn. The theoretical radiation patterns are compared with the cold test and HPM experimental results.

2. OPTIMIZATION OF THE HPM FEED HORN AND DIELECTRIC WINDOW

2.1. The Reference of the Uniform Aperture Field

For linear polarization of the exciting TE_{11} mode, reference is missing for scaling the amplitude of the aperture field of the horn. It has been found by simulation and theoretical calculation that the field amplitude E_{m0} of TE_{11} mode is usually lower than that of the multimode in a uniform waveguide of the same cross-section. For instance, E_{m0} of TE_{11} mode is the minimum value within the modes of TM_{11}, TE_{12}, TM_{12}, and TE_{13}. The transversal electric field of the fundamental Gaussian beam can be mainly expressed by that of the mixture mode of TE_{11} and TM_{11} with amplitude ratio $1:0.65$ and phase $0:180$ [23]. It has been found by calculation that the amplitude of the transversal field of the mixed mode is higher than that of the single TE_{11} mode.

Thereby, the amplitude of TE_{11} mode in a waveguide with the same diameter can be used as the reference for scaling the aperture-field uniformity of the multimode horn. Define the ratio factor $\gamma = E_m/E_{m0}$, where E_m is the aperture-field amplitude of the horn.

For $D/\lambda \gg 1$, the longitudinal phase-shift constant meets $\beta = \sqrt{\omega^2/c^2 - 1.841/R)^2} \approx \omega/c$, E_{m0} can be approximately expressed as:

$$E_{m0} \approx 1.632\sqrt{P_{TE11}c\mu}/R \tag{1}$$

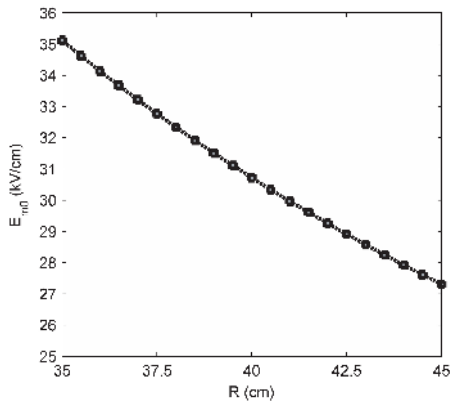

Figure 1. Variation of E_{m0} with radius R for $P_{TE11} = 3\,\mathrm{GW}$.

where P_{TE11} is the incident power, and it can be shown that E_{m0} is independent of frequency ω. Variation of E_{m0} for $P_{TE11} = 3\,\mathrm{GW}$ is illustrated in Fig. 1.

It's shown in Fig. 1 that E_{m0} at $R = 40.5\,\mathrm{cm}$ is $30\,\mathrm{kV/cm}$, below the breakdown threshold. Thus, the aperture radius of the flared horn for 4.3 GHz is chosen as 40.5 cm, satisfying $D/\lambda \gg 1$.

2.2. Simulation and Optimization of the Feed Horn

The schematic of the structure of the flared feed horn is shown in Fig. 2. In the simulation with CST Microwave Studio, the polarization direction of the exciting TE_{11} mode is along y-axis and the wave propagation direction is along z-axis. The optimization goals are uniform aperture field, equal 10 dB beamwidth (BW) in the principal planes. The aperture field and radiation patterns are influenced by the three structure variables (L_1, L_2, and R_1), since the aperture radius R_2 has been determined in the analysis above, and the incident R_0 is fixed due to the output waveguide of the HPM source. In order to simplify the problem, a single variable is firstly investigated to research its influence on the optimization goals while fixing other parameters. And then, another variable is optimized.

The parameters for simulation in CST are $f = 4.3\,\mathrm{GHz}$, $R_0 = 44.5\,\mathrm{mm}$, $R_2 = 405\,\mathrm{mm}$, incident average power $P_{TE11} = 0.5\,\mathrm{W}$, and the optimized field $E_{m0} = 40\,\mathrm{V/m}$ for 0.5 W.

During the process of respectively optimizing the three parameters, it was found that the length of L_2 has the largest influence on aperture field and radiation patterns. Optimizing the variables of R_1 and L_1 can further decrease the field amplitude, make the patterns symmetric and form low sidelobes.

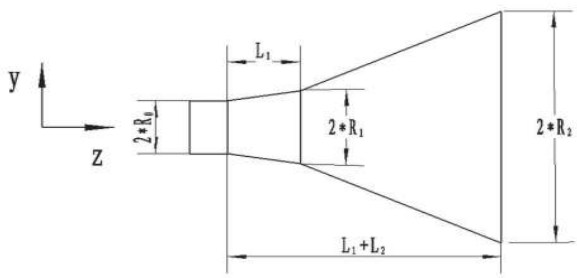

Figure 2. The schematic of the structure of the two-time flared feed horn.

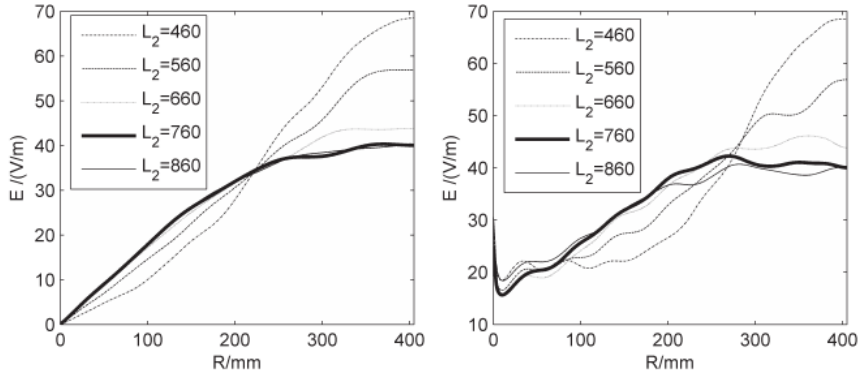

Figure 3. Aperture field distribution with L_2 along (a) x-axis and (b) y-axis paralleled with polarization direction of TE_{11}.

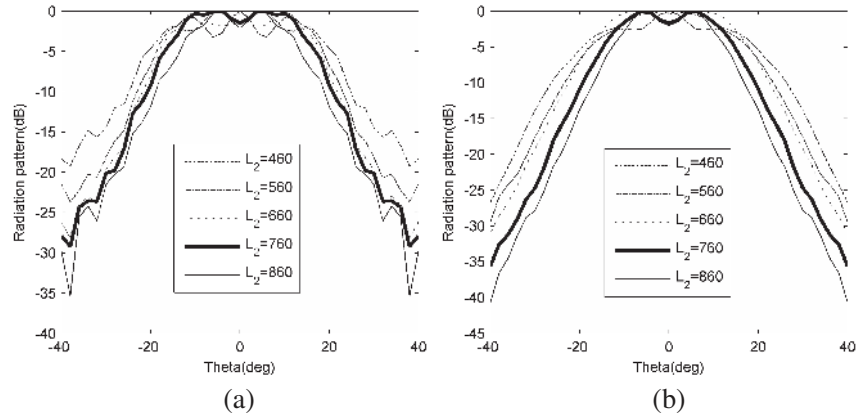

Figure 4. Radiation patterns with L_2 for (a) E plane and (b) H plane.

Firstly, fix $L_1 = 200\,\text{mm}$ and $R_1 = 80\,\text{mm}$, and vary L_2. It was discovered that, when the secondary flared angle θ_2 is in the range of 40–90°, the field amplitude keeps very high, therefore, θ_2 can be selected in the range of 20–35°, corresponding to $L_2 = 460$–$860\,\text{mm}$. Variation of aperture field and radiation patterns in the E and H principle planes with L_2 are shown in Fig. 3 and Fig. 4.

It can be observed in Fig. 3 that, with the increase of L_2, the field distribution becomes uniform and the amplitude gradually decreases; the 10 dB-BW in the H plane gets narrower and tends to be equal

with that in the E plane. Combining the results of aperture field and radiation patterns, $L_2 = 760\,\text{mm}$ can be selected as the optimized value. And then, the influence of L_1 can be investigated, primary optimization shows that relatively good results can be obtained for $\theta_1 = 4$–$8°$, corresponding to $L_1 = 150$–$270\,\text{mm}$. Variation of aperture field and radiation patterns with L_1 are shown in Fig. 5 and Fig. 6.

With the increase of L_1, the field amplitude gradually enhances, the 10 dB-BW of the E plane gets narrower and tends to be equal with that of the H plane. $L_1 = 220\,\text{mm}$ can be selected as the optimized value, and then the influence of R_1 can be investigated. The results are shown in Fig. 7 and Fig. 8.

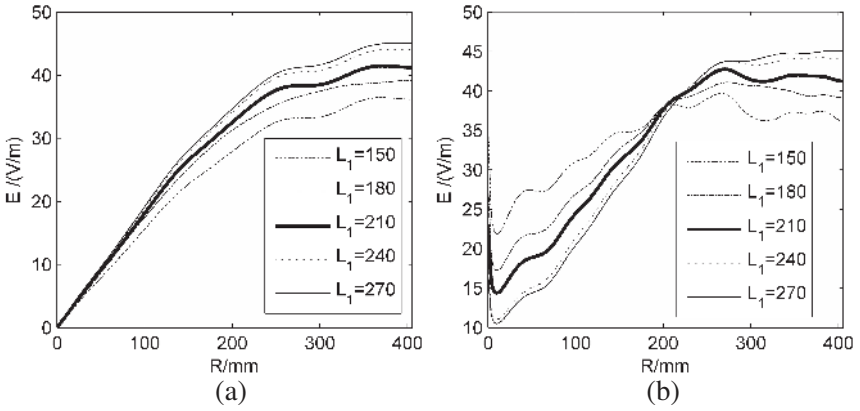

Figure 5. Aperture field distribution with L_1 along (a) x-axis and (b) y-axis.

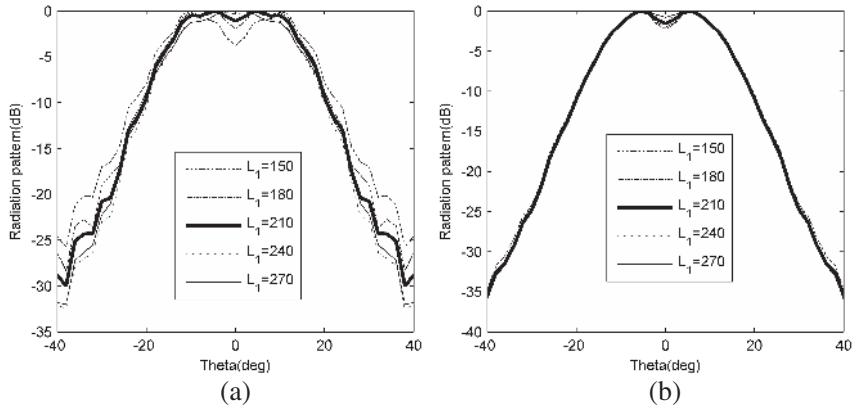

Figure 6. Radiation patterns with L_1 for (a) E plane and (b) H plane.

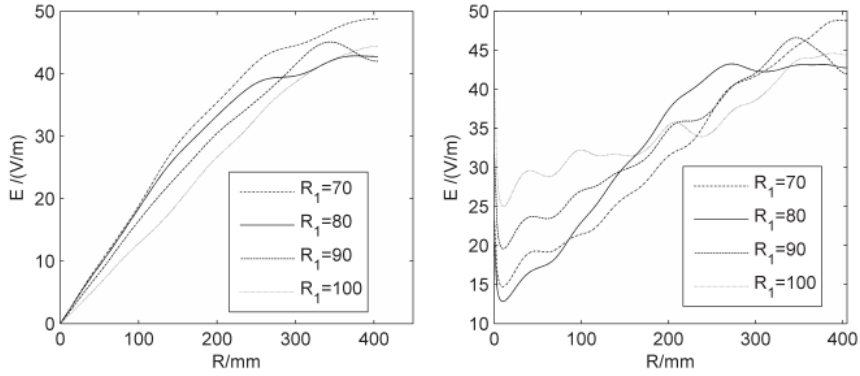

Figure 7. Aperture field distribution with R_1 along (a) x-axis and (b) y-axis.

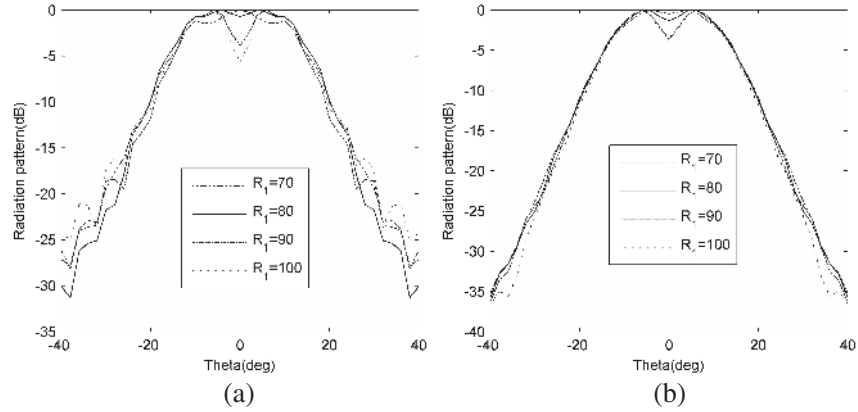

Figure 8. Radiation patterns with R_1 for (a) E plane and (b) H plane.

It is illustrated that relative good patterns and aperture field can be acquired at $R_1 = 80$ mm, and the ratio $\gamma = E_m/E_{m0}$ is 1.1. When R_1 is increasing, aperture field E improves and concave emerges at the top of the radiation beam. During optimizing the structure parameters (L_2, L_1, and R_1), appropriate phase center region has been considered, which is mainly determined by the reflector antenna and is about 860 mm away from the aperture of the horn.

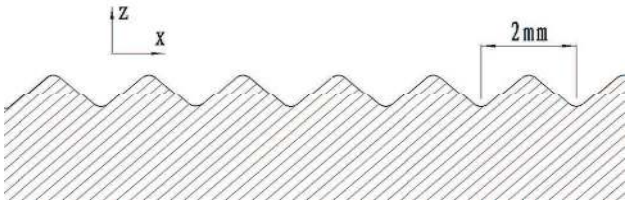

Figure 9. Schematic of the periodic triangular surface.

2.3. Optimization of the Dielectric Window

The dielectric window with $\Phi \sim 0.8\,\mathrm{m}$, isolating vacuum from air, should have sufficiently mechanical strength to withstand the huge atmospheric pressure. Besides, in order to minimize microwave reflection, the thickness of the window should satisfy $d = n\lambda/(2\varepsilon_r^{0.5})$, where λ is the wavelength, ε_r is the dielectric constant, and n is a positive integer.

Periodic rectangular and triangular surface profiles with period $p \sim 2\,\mathrm{mm}$ have been found to increase the breakdown threshold of dielectric window at the vacuum side, by the theoretical analysis and recent HPM experiments [27, 28].

Spherical shell dielectric window has been replaced by the flat one due to very expensive grooving on the curved surface. For high molecular weight polyethylene (HMWPE) with $\varepsilon_r = 2.3$ for 4.3 GHz, the thickness of the window is chosen as $d \sim 69\,\mathrm{mm}$. The HMWPE window has been processed to be periodic triangular surface with slope angle 45° and period $p \sim 2\,\mathrm{mm}$ shown in Fig. 9, which has little effect on microwave transmission due to $p \ll \lambda \sim 7\,\mathrm{cm}$.

2.4. The Results of the Optimization

The parameters of the optimized HPM feed horn and dielectric window in C band is shown in Table 1:

Table 1. The parameters of the optimized HPM feed horn.

R_0 /mm	R_1	R_2	L_1	L_2	HMWPE d/mm	10 dB-BW/°	Gain/dB	γ	E_m for 3 GW kV/cm
44.5	80	405	220	760	69	40	18	1.14	33.5

The influence of the optimized dielectric window on radiation patterns, and aperture field shown Fig. 11 and Fig. 12 is not serious and the ratio $\gamma = 1.14$ illustrates that the aperture field is relatively

uniform. The transient field distribution of the horn under 0.5 W is shown in Fig. 10. It can be observed in Figs. 12(a) and (b) that the mainlobe is symmetric on the whole, and low sidelobes beneath −40 dB are satified. The nearfield and the farfield patterns are found to be the same except for the amplitude and phase in the simulation. Thus, the nearfield patterns are not plotted. The total length of the compact horn including dielectric window is 1.05 m, shown in Table 1.

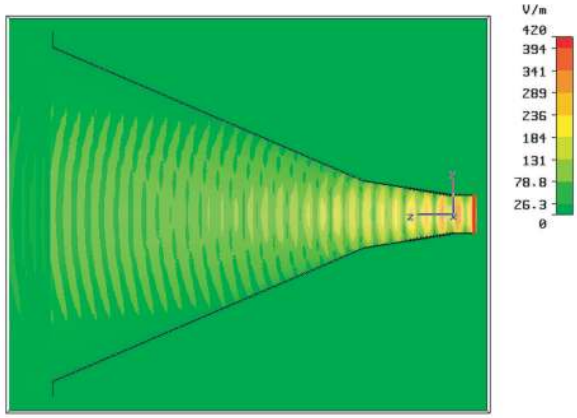

Figure 10. Distribution of E-field in y-z plane for average 0.5 W.

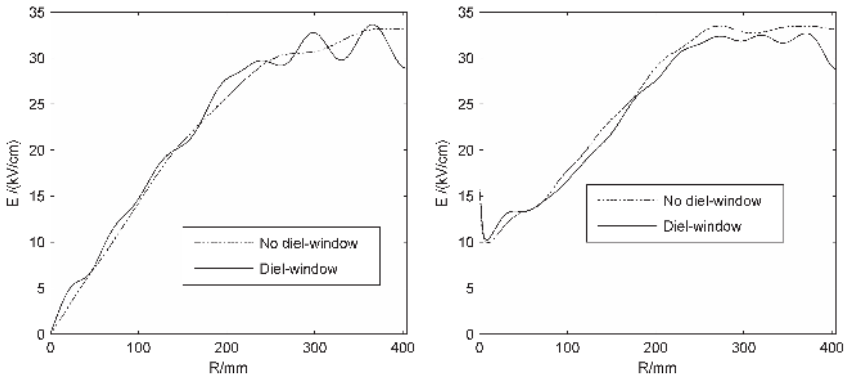

Figure 11. Comparison of the aperture field distribution with and without dielectric window along (a) x-axis and (b) y-axis for 3 GW incident power.

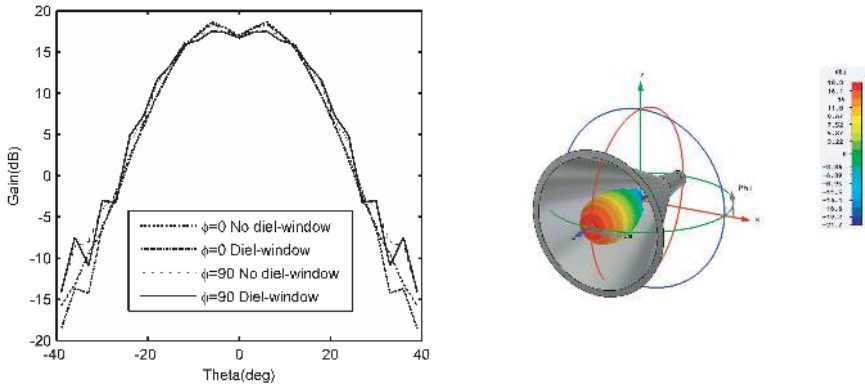

(a) (b)

Figure 12. (a) Farfield radiation patterns with and without dielectric window for E plane ($\phi = 90°$) and H plane ($\phi = 0°$). (b) 3D farfield radiation patterns.

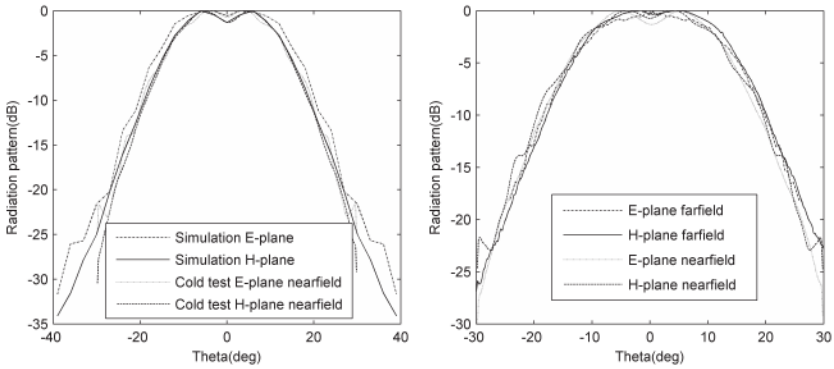

(a) (b)

Figure 13. (a) Comparison of the theoretical and cold-test nearfield patterns. (b) Comparison of the cold-test nearfield and farfield patterns.

3. COLD TESTS

Cold tests of the farfield and nearfield radiation patterns of the feed horn without the dielectric window were conducted in a huge microwave anechoic chamber. The test system comprised sending and receiving components according to the principle of reciprocity of the antenna. The sending subsystem was comprised of signal source Agilent E8247C, directional coupler HP87300C, and transmit antenna.

The reception subsystem was constituted by the testing feed horn cooperated with TM_{01}-mode exciter and mode convertor from TM_{01} to TE_{11}, frequency inverter Agilent 85320A/B, vector network analyzer Agilent E8363B, and scanning antenna mount (or turntable). The cold-test patterns for nearfield of 1.5 m and farfield are compared with the theoretical ones in Figs. 13(a) and (b).

It can be observed in Fig. 13(a) that the theoretical and cold-test patterns in E-plane are slightly different. Besides, the cold-test patterns of nearfield and farfield are a little different in shape, in contrast with their theoretical predictions that are in close agreement. The possible reason may be that the impure and non-single output modes of the mode convertor may excite higher order modes in the horn, influencing the radiation field.

The gain measured by comparison method using a standard gain antenna was 18.22 dB, in agreement with the theoretical value. And the phase center region measured was also consistent with the theoretical one.

4. HPM EXPERIMENTS AND RESULTS

HPM experiment, with power 3 GW and 25–30 ns pulse width, and at frequency 4.3 GHz, was conducted. The experimental set up is shown in Fig. 14. TM_{01} mode produced by BWO [29] was transferred by the mode convertor to TE_{11} mode, which was radiated to air through the two-time flared circular horn with HMWPE window grooved periodically, and the inner pressure 0.1 mTorr was acquired by mechanical pump and molecular pump. SF_6 with pressure higher than 1atm. was sealed in a balloon with diameter 1.5 m and fixed outside of the window to prevent air breakdown.

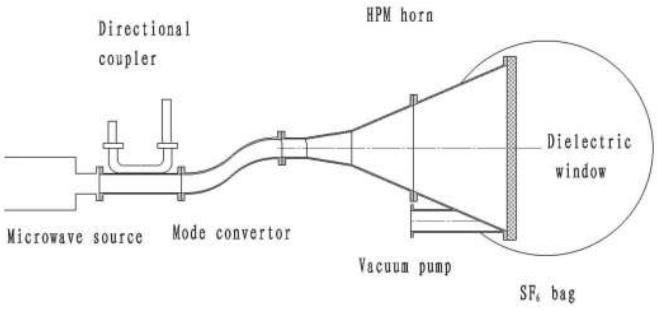

Figure 14. Basic HPM experiment setup.

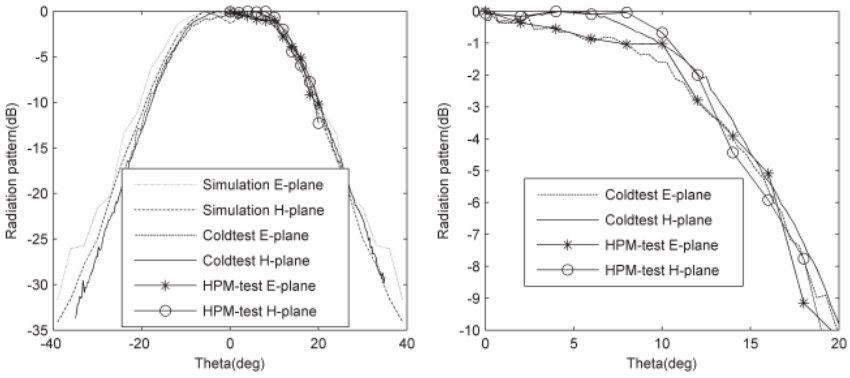

(a) (b)

Figure 15. (a) Comparison of the radiation patterns of the theoretical calculation, cold test and HPM test. (b) The local amplified patterns for cold test and HPM test.

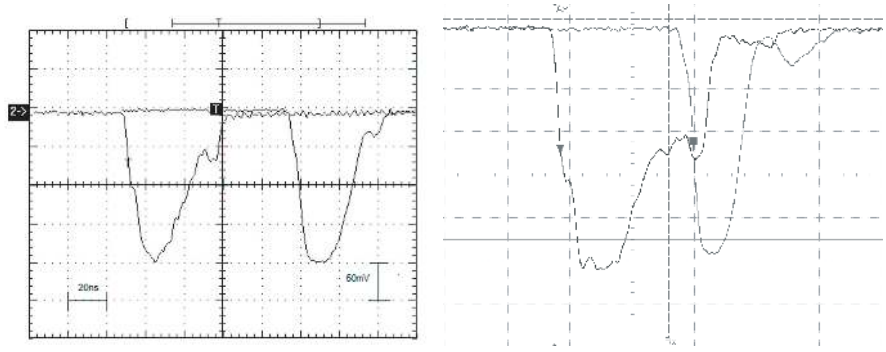

(a) (b)

Figure 16. Typical waveforms for (a) no breakdown (b) breakdown for, left- incident microwave power, right-radiation power.

Directional couplers, attenuators, coaxial transmission lines, and crystal diode detectors were adopted to measure the online incident microwave power and radiation power tested (not shown in Fig. 14) at a distance 9 m from the phase center of the horn.

The received power of the detector for online measurement was attenuated by about 120 dBmW, which was the sum of directional coupler, attenuators and coaxial transmission line. The detector transformed the input power (unit of dBmW) to output voltage (mV), whose relation curve had been calibrated by standard microwave source. The output voltage was measured by oscillograph. The

theoretical, cold-test and HPM-test radiation patterns are compared in Fig. 15.

It is illustrated in Fig. 15(b) that the cold-test radiation patterns are basically consistent with the HPM patterns, whose integrated power is higher than 3 GW. The typical waveform of the incident HPM power higher than 3 GW and the corresponding radiation power is shown in Fig. 16(a). As a comparison, the breakdown waveform of the radiation wave came from a smaller size horn with much higher aperture field is illustrated in Fig. 16(b). When breakdown happens, the transmitted pulse obviously shortens, that is to say, the radiation pulse width gets shorter than the incident one, shown in Fig. 16(b).

5. CONCLUSION

Theoretical design, cold tests and HPM experiments were adopted to investigate the HPM feed horn. By combining the aperture field with radiation patterns, the compact HPM feed horn in C band is optimized and satisfies relatively uniform aperture field, power capacity higher than 3 GW demonstrated by HPM experiment, and symmetric radiation patterns, which for theoretical analysis is basically consistent with the cold-test and HPM experimental results.

REFERENCES

1. Korovin, S., I. Kurkan, S. Loginov, I. Pegel, S. Polevgin, S. Volkov, and A. Zherlitsyn, "Decimeter-band frequency-tunable sources of high-power microwave pulses," *Laser Part. Beams*, Vol. 21, No. 2, 175–185, 2003.
2. Neuber, A., M. Butcher, H. Krompholz, L. Hatfield, and M. Kristiansen, "The role of outgassing in surface flashover under vacuum," *IEEE Trans. Plasma Sci.*, Vol. 28, No. 5, 1593–1598, 2000.
3. Chang, C., G. Liu, C. Tang, C. Chen, and S. Qiu, "The influence of desorption gas to high power microwave window multipactor," *Phys. Plasmas*, Vol. 15, No. 9, 093508, 2008.
4. Chang, C., G. Liu, X. Zhu, H. Chen, and J. Fang, "Improved model for window breakdown at low pressure," *Phys. Plasmas*, Vol. 16, No. 3, 033505, 2009.
5. Chang, C., G. Liu, C. Tang, and L. Yan, "The influence of space charge shielding on dielectric multipactor," *Phys. Plasmas*, Vol. 15, No. 5, 053506, 2009.

6. Neuber, A., L. Laurent, Y. Lau, and H. Krompholz, *High Power Microwave Sources and Technologies*, R. J. Barker and E. Schamiloglu (eds.), Chap. 10, IEEE, Piscataway, NJ, 2001.
7. Olver, A., P. Clarricoats, A. Kishk, and L. Shafai, *Microwave Horns and Feeds*, The Institute of Electrical and Electronics Engineers, Inc., New York, 1994.
8. Balanis, C. A., *Antenna Theory Analysis and Design*, 2nd edition, John Wiley & Sons, Inc., New York, 2005.
9. Volakis J., R. Johnson, and H. Jasik, *Antenna Engineering Handbook*, MC Graw Hill, Inc., New York, 2007.
10. Green, H. E., "The radiation pattern of a conical horn," *Journal of Electromagnetic Waves Applications*, Vol. 20, No. 9, 1149–1160, 2006.
11. Kishk, A. A. and C.-S. Lim, "Comparative analysis between conical and Gaussian profiled horn antenns," *Progress In Electromagnetic Research*, PIER 38, 147–166, 2002.
12. Agastra, E., G. Bellaveglia, L. Lucci, R. Nesti, G. Pelosi, G. Ruggerini, and S. Selleri, "Genetic algorithm optimization of high-efficiency wide-band multimodal square horns for discrete lenses," *Progress In Electromagnetic Research*, PIER 83, 335–352, 2008.
13. Lee, K. and R. Chu, "Design and analysis of a multimode feed horn for a monopulse feed," *IEEE Trans. Antennas Propagat.*, Vol. 36, No. 2, 171–181, 1988.
14. Yin, X. H. and S. C. Shi, "A simple design method of multimode horns," *IEEE Trans. Antennas Propagat.*, Vol. 53, No. 1, Part 2, 455–459, 2005.
15. Bhattacharyya, A. K. and G. Goyette, "A novel horn radiator with high aperture efficiency and low cross-polarization and applications in arrays and multibeam reflector antennas," *IEEE Trans. Antennas Propagat.*, Vol. 52, No. 11, 2850–2859, 2004.
16. Kildal, P. S., "Artificially soft and hard surfaces in electromagnetic," *IEEE Trans. Antennas Propagat.*, Vol. 38, No. 10, 1537–1544, 1990.
17. Gupta, R. C. C. and S. P. Singh, "Development and analysis of a microwave direct contact water-loaded box-horn applicator for therapeutic heating of bio-medium," *Progress In Electromagnetics Research*, PIER 62, 217–235, 2006.
18. Gupta, R. C. C. and S. P. Singh, "Analysis of radiation patterns of compound box-horn antenna," *Progress In Electromagnetics Research*, PIER 76, 31–44, 2007.

19. Yu, J., M. Yuan, and Q. H. Liu, "A wideband half oval patch antenna for breast imaging," *Progress In Electromagnetics Research*, PIER 98, 1–13, 2009.
20. Dehdasht-Heydari, R., H. R. Hassani, and A. R. Mallahzadeh, "A new 2–18 GHz quad-ridged horn antenna," *Progress In Electromagnetic Research*, PIER 81, 183–195, 2008.
21. Dehdasht-Heydari, R., H. R. Hassani, and A. R. Mallahzadeh, "Quad ridged horn antenna for UWB applications," *Progress In Electromagnetic Research*, PIER 79, 23–38, 2008.
22. Mallahzadeh, A. R. and F. Karshenas, "Modified TEM horn antenna for broadband applications," *Progress In Electromagnetic Research*, PIER 90, 105–119, 2009.
23. Li, H., J. Li, H. Wang, T.-M. Li, and Y.-H. Zhou, "Design of the high efficiency circular horn feed for high-power microwave system," *Progress In Electromagnetic Research C*, Vol. 8, 1–12, 2009.
24. Green, H., "The phase centre of a pure mode, smooth wall, conical horn," *Progress In Electromagnetics Research B*, Vol. 4, 285–298, 2008.
25. Fazaelifar, M. and M. Fatorehchy, "Design, fabrication and test of parabolic cylinder reflector and horn for increasing the gain of vlasov antenna," *Progress In Electromagnetics Research Letters*, Vol. 4, 191–203, 2008.
26. ST Microwave Studio, Germany, http://www.cst.com.
27. Chang, C., H. Huang, G. Liu, C. Chen, Q. Hou, J. Fang, X. Zhu, and Y. Zhang, "The effect of grooved surface on dielectric multipactor," *J. Appl. Phys.*, Vol. 105, No. 12, 123305, 2009.
28. Chang C., G. Liu, H. Huang, C. Chen, and J. Fang, "Suppressing high-power microwave dielectric multipactor by the sawtooth surface," *Phys. Plasmas*, Vol. 16, No. 8, 083501, 2009.
29. Xiao, R. Z., C. H. Chen, X. W. Zhang, and J. Sun, "Efficiency enhancement of a high power microwave generator based on a relativistic backward wave oscillator with a resonant reflector," *J. Appl. Phys.*, Vol. 105, No. 5, 053306, 2009.